1-1-1996

# A Model for the Galvanostatic Deposition of Nickel Hydroxide

Mahesh Murthy
*University of South Carolina - Columbia*

Gowri S. Nagarajan
*University of South Carolina - Columbia*

John W. Weidner
weidner@engr.sc.edu

John W. Van Zee
*University of South Carolina - Columbia*, vanzee@engr.sc.edu



## Publication Info

*Journal of the Electrochemical Society*, 1996, pages 2319-2327.

Publisher's link: http://dx.doi.org/10.1149/1.1837000
DOI: 10.1149/1.1837000

# A Model for the Galvanostatic Deposition of Nickel Hydroxide

**Mahesh Murthy,* Gowri S. Nagarajan,* John W. Weidner,** and J. W. Van Zee****

*Department of Chemical Engineering, University of South Carolina, Columbia, South Carolina 29208, USA*

ABSTRACT

A mathematical model is presented for the galvanostatic deposition of $Ni(OH)_2$ films in stagnant $Ni(NO_3)_2$ solutions. The objective is to quantify the anomalous deposition behavior reported previously in which the utilization of the electrochemically generated $OH^-$ species decreased drastically as the concentration of $Ni(NO_3)_2$ increased beyond 0.1 *M*. For example, as the $Ni(NO_3)_2$ concentration increased from 0.1 to 2.0 *M*, the deposition rate decreased by a factor of ten at 2.5 mA/cm$^2$. At this high ratio of concentration to current density, a comparison with Faraday's law indicates that only 10% of the $OH^-$ species generated at the surface led to deposition. It has been proposed that the inefficient use of electrochemically generated $OH^-$ species is due to the presence of $Ni_4(OH)_4^{4+}$ as an intermediate in the deposition process. As the bulk $Ni(NO_3)_2$ concentration increases, the concentration of $Ni_4(OH)_4^{4+}$ at the electrode surface increases. A high concentration of the intermediate results in an increase in the diffusion rate of the species away from the electrode surface and thus a decrease in the deposition rate. Here, this hypothesis is tested by developing a model which includes the generation of $OH^-$ from the electrochemical reduction of nitrate to ammonia and the diffusion and migration of $Ni^{2+}$, $NO_3^-$, $OH^-$, $H^+$, and $Ni_4(OH)_4^{4+}$. The model predictions agree well with previously reported mass deposition data collected using an electrochemical quartz crystal microbalance at different currents and over a range of $Ni(NO_3)_2$ concentrations. The present work confirms the role that $Ni_4(OH)_4^{4+}$ plays in the deposition process and provides a fundamental framework for understanding the electrochemical impregnation of nickel electrodes.

## Introduction

Electrochemical impregnation is one of the main processes for the production of nickel hydroxide electrodes, because it yields superior electrodes with longer life.[1] This process involves the electrochemical reduction of $NO_3^-$ within a porous nickel sinter and the subsequent generation of $OH^-$. Although any or all of reactions I-1 through I-5 shown in Table I could be involved, the primary result is the production of $OH^-$, which may react further with $Ni^{2+}$ species to form $Ni(OH)_2$ according to reaction I-6. Recently, Streinz *et al.*[2] reported the anomalous deposition behavior of $Ni(OH)_2$ wherein they observed a drastic decrease in deposition rates as $Ni(NO_3)_2$ concentration increased from 0.1 to 2.0 *M*. They measured deposition rates for different currents and $Ni(NO_3)_2$ concentrations using an electrochemical quartz crystal microbalance (EQCM). In 2.0 *M* $Ni(NO_3)_2$ solutions, they observed only 10% utilization of the electrochemically generated $OH^-$ species, as compared to almost 100% utilization in 0.1 *M* solutions at 2.5 mA/cm$^2$. They concluded that the diffusion of an intermediate, $Ni_4(OH)_4^{4+}$ species was responsible for this inefficiency. Baes and Mesmer[3] also mention that for high $Ni^{2+}$ concentrations ($C_{Ni^{2+}} > 0.1$ *M*), the $Ni_4(OH)_4^{4+}$ species is formed predominantly. Based on these observations, Streinz *et al.*[2] postulated a two-step deposition mechanism shown by reactions I-7 and I-8. The deposition occurs at the surface of the electrode which is saturated in hydroxyl ions and where the pH is between 6.5 and 8. The pH at which deposition begins is a strong function of $Ni(NO_3)_2$ concentration, as shown in Fig. 1a.

* Electrochemical Society Student Member.
** Electrochemical Society Active Member.

Figure 1a shows that pH affects the equilibrium distribution of nickel species for reactions I-7 through I-11. (The calculations used for this figure are discussed in Appendix A.) The pH at which $Ni(OH)_2$ forms decreases from 7.2 for 0.5 *M* $Ni(NO_3)_2$ to 6.8 for 4 *M* solutions. Figure 1a also shows that, in 4 *M* solutions, about 75% of the nickel exists as $Ni_4(OH)_4^{4+}$ prior to the deposition of $Ni(OH)_2$. This maximum decreases to 65 and 40% for 2 and 0.5 *M* solutions, respectively. Figure 1a shows that at a pH less than 5 almost all the nickel exists as its divalent ion. These calculations are consistent with our measurements of the pH for various temperatures and concentrations of $Ni(NO_3)_2$ shown in Fig. 1b. (See Appendix B for a discussion of the experimental technique.)

Figure 1b shows that the pH of $Ni(NO_3)_2$ solutions drops from 3.75 for 0.5 *M* to 1.2 for 4.0 *M* (at 25°C). A similar trend is also observed at higher temperatures. The change in pH is attributed to the generation of $H^+$ mainly due to the formation of hydrolysis products like $NiOH^+$ according to reaction I-11. We calculate that, for 4.0 *M* solutions, about 2% of $Ni^{2+}$ is bound to $OH^-$ generated from the water equilibrium reaction, and this results in a pH of 1.2. However, this value is difficult to see on the scale in Fig. 1a. Note that a comparison of the equilibrium constants for reactions I-10 and I-7 indicates that the concentration of $NiOH^+$ is small in the region where $Ni_4(OH)_4^{4+}$ exists.

The purpose of this paper is to test the hypothesis of Streinz *et al.*[2] by developing a model and comparing the predictions with their experimental results. Other workers[4-6] have deposited films on planar electrodes but made no attempt to quantify the deposition process over a range of deposition conditions. For example, Cordoba-Torresi

**Table I. Electrochemical and chemical reactions considered in the model. (All values correspond to standard conditions at 25°C.)**

| | | |
|---|---|---|
| $NO_3^- + H_2O + 2e^- \rightarrow NO_2^- + 2\ OH^-$ | $U^0 = 0.01$ V | [I-1][a] |
| $NO_3^- + 5H_2O + 6e^- \rightarrow NH_3 + 7\ OH^-$ | $U^0 = -0.165$ V | [I-2][a] |
| $NO_3^- + 6H_2O + 8e^- \rightarrow NH_3 + 9\ OH^-$ | $U^0 = -0.12$ V | [I-3][a] |
| $2NO_2^- + 4H_2O + 6e^- \rightarrow N_2 + 8\ OH^-$ | $U^0 = 0.406$ V | [I-4] |
| $2NO_2^- + 3H_2O + 4e^- \rightarrow N_2O + 6\ OH^-$ | $U^0 = 0.15$ V | [I-5] |
| $Ni^{2+} + 2\ OH^- \leftrightarrow Ni(OH)_2\downarrow$ | $K_{sp,6} = 1.6 \times 10^{-23}$ (mol/cm$^3$)$^3$ (see Ref. 12) | [I-6] |
| $Ni^{2+} + OH^- \leftrightarrow 1/4\ Ni_4(OH)_4^{4+}$ | $K_{eq} = 2.63 \times 10^{12}$ (mol/cm$^3$)$^{-7/4}$ [c] | [I-7] |
| $1/4\ Ni_4(OH)_4^{4+} + OH^- \leftrightarrow Ni(OH_2)\downarrow$ | $K_{sp} = 3.3 \times 10^{-11}$ (mol/cm$^3$)$^{5/4}$ [b] | [I-8] |
| $H^+ + OH^- \leftrightarrow H_2O$ | $K_W = 1 \times 10^{-20}$ (mol/cm$^3$)$^2$ | [I-9] |
| $Ni^{2+} + OH^- \leftrightarrow NiOH^+$ | $K_{10} = 1.38 \times 10^7$ cm$^3$/mol [d] | [I-10] |
| $Ni^{2+} + H_2O \leftrightarrow NiOH^+ + H^+$ | $K_{11} = 1.38 \times 10^{-13}$ mol/cm$^3$ (see Ref. 13) | [I-11] |

[a] Equation I-3 used in the model is a combination of I-1 and I-2.
[b] Calculated from $K_{sp,6}$ and $K_{eq}$ of reactions I-6 and I-7.
[c] Calculated by using $K_W$ and reported value of log $K_{eq} = -27.32$ from Ref. 9.
[d] Calculated using $K_W$ and $K_{11}$.

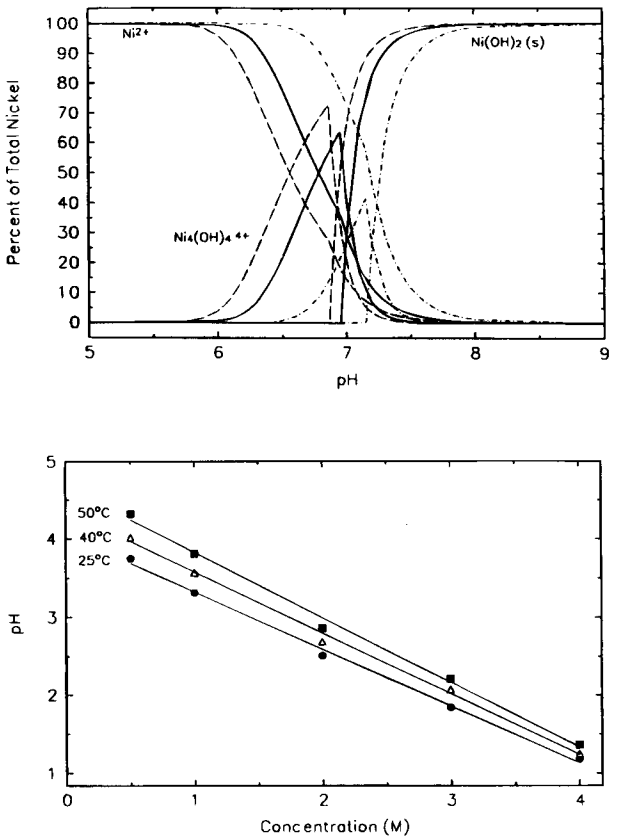


**Fig. 1. (a, top) Equilibrium distribution of hydrolysis products for 4 (– –), 2 (—), and 0.5 *M* (– · –) $Ni(NO_3)_2$ solutions. The ordinate represents the percent of nickel existing as $Ni^{2+}$, $Ni_4(OH)_4^{4+}$, or as $Ni(OH)_2$. The concentration of $Ni_4(OH)_4^{4+}$ prior to deposition is proportional to $Ni(NO_3)_2$ concentration. For 4 *M* $Ni(NO_3)_2$, almost 75% of the total nickel exists as $Ni_4(OH)_4^{4+}$ in the pH range prior to deposition. This decreases to 65% for 2 *M* and 40% for 0.5 *M* solutions. Thus, the concentrations of $Ni_4(OH)_4^{4+}$ are 0.75, 0.325, or 0.05 *M*, respectively. (b, bottom) pH of aqueous $Ni(NO_3)_2$ solutions as a function of temperature. The solid lines show a good linear dependence. The pH of the solutions decreases with an increase in $Ni(NO_3)_2$ concentration due to the formation of hydrolysis products.**

*et al.*[4] deposited $Ni(OH)_2$ films from dilute solutions using a quartz-crystal microbalance to study its electrochromic behavior. Pickett and Maloy[5] codeposited $Co(OH)_2$ in $Ni(OH)_2$ films and quantified its effects during cycling. MacArthur[6] postulated that proton diffusion was the rate-controlling process during the oxidation and reduction of films. Bernardi,[7] on the other hand, studied the kinetics of nitrate reduction using a rotating-disk assembly and developed a model for $Ni(OH)_2$ film formation based on the single-step deposition of reaction I-6 and the electrochemical production of $HNO_2$. The model developed in this paper considers the diffusion and migration of $Ni^{2+}$, $NO_3^-$, $OH^-$, $H^+$, and $Ni_4(OH)_4^{4+}$ at a planar electrode. The model predictions agree well with the mass-deposition data of Streinz *et al.*[2] for a range of current densities and $Ni(NO_3)_2$ concentrations.

## Mathematical Model

Figure 2 shows the scheme of the EQCM electrode surface with the growing film. The flux of the $Ni_4(OH)_4^{4+}$ species is directed away from the electrode surface, indicating that diffusion or migration of this species into the bulk can occur before deposition. A growing diffusion layer is characteristic of this experimental system, and this diffusion layer is approximately 100 times larger than the thickness of the deposit.

The equations that describe the deposition mechanism of nickel hydroxide are derived by considering Fig. 2 and

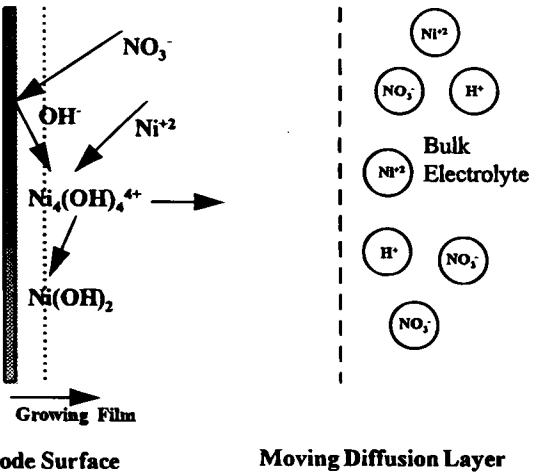


**Fig. 2. Scheme of the deposition process on planar electrodes. The nickel in the solution complexes with the electrochemically generated $OH^-$ and may diffuse into the bulk prior to precipitation.**

the dilute-solution theory described by Newman.[8] The dependent variables of interest are the five ionic species, numbered 1 to 5: $Ni^{2+}$, $NO_3^-$, $H^+$, $OH^-$, and $Ni_4(OH)_4^{4+}$, and the solution potential, $\phi$. The assumptions used to model the conditions during EQCM experiments concerned with the growth of $Ni(OH)_2$ films are:

1. One-dimensional transport is considered in the direction normal to the surface of the electrode.
2. Dilute-solution theory applies.
3. The electrolyte is stagnant during deposition. Therefore, the flux of all species is purely due to diffusion and migration.
4. Isothermal conditions exist.
5. The thickness of the film is much smaller than that of the diffusion layer. Therefore, there is no spatial difference between the electrode surface where $OH^-$ is produced and the front of the film where $Ni(OH)_2$ is deposited. The film is slightly porous to allow $OH^-$ transport from the electrode to the deposition site.
6. The volume of the deposition bath is large relative to the electrode area so that the concentration of $Ni(NO_3)_2$ is assumed to remain constant during deposition.
7. The electrochemical reaction of nitrate reduction occurs according to the stoichiometry of reaction I-3 and without nitrite or nitrous acid intermediates.
8. Deposition of $Ni(OH)_2$ occurs only at the electrode surface with no bulk precipitation. The film is assumed to be composed of pure $Ni(OH)_2$.
9. The vertical length of the EQCM electrode is small so that natural convection is negligible.
10. Activity coefficient corrections to the equilibrium and solubility product constants are negligible.
11. The concentration of $NH_3$ is small, and $NH_4^+$ and nickel-ammonia complexes are not important.

The concentration of each ionic species is governed by the following material-balance equation

$$\frac{\partial C_i}{\partial t} = -\nabla \cdot N_i + R_i \quad (i = 1, 2, 3, 4, 5) \qquad [1]$$

where $R_i$ denotes the net homogenous production of species i from all reactions. Therefore, $R_i = \Sigma r_{ij}$ (i-species, j-reaction) where $r_{ij}$ refers to the homogenous production rate of species i in individual reactions. The flux of each species is given by

$$N_i = -D_i \frac{\partial C_i}{\partial x} - \frac{z_i D_i F C_i}{RT} \frac{\partial \phi}{\partial x} \qquad [2]$$

and contains contributions from diffusion and migration only. The potential in the solution varies according to the electroneutrality condition

$$\Sigma z_i C_i = 0 \qquad [3]$$

The homogenous reaction rate can be written explicitly for each species according to Eq. 4. The numbered subscripts in Eq. 4 refer to the specific reaction number in Table I.

$$R_1 = r_{1,7} \quad R_2 = 0 \quad R_3 = r_{3,9}$$
$$R_4 = r_{4,7} + r_{4,9} \quad R_5 = r_{5,7} \qquad [4]$$

Equation 1 with $i = 1$ to 5 results in five material-balance expressions with species 1, 3, 4, and 5 each containing a homogenous reaction term. The unknown rates can be eliminated by combining the expressions in Eq. 1, suitably resulting in three equations. These three equations and two equilibrium expressions (Eq. I-7 and I-9) form the governing equations listed in Table IIA as Eq. II-7 through II-11.

*Boundary conditions at the diffusion layer-electrolyte interface.*—The boundary conditions far from the surface correspond to bulk conditions where the equilibrium relations are valid. Therefore, as shown in Eq. II-1 through II-6 of Table IIA, at $x = \infty$. The initial conditions are

$$C_1 = \frac{1}{2} C_2^o$$
$$C_2 = C_2^o$$
$$C_3 = C_3^o$$
$$C_4 = \frac{K_W}{C_3^o} \qquad [5]$$
$$C_5 = (K_{eq} C_1 C_4)^4$$
$$\phi = 0$$

where $C_2^o$ is the bulk concentration of $NO_3^-$ species and $C_3^o$ is the concentration of $H^+$ corresponding to the experimentally measured pH at the specified bulk $NO_3^-$ concentration.

*Boundary conditions at the electrode surface.*—The boundary conditions at the electrode surface depend on pH and whether deposition of $Ni(OH)_2$ occurs, as shown in Table IIB. Common to both sets are the equations corresponding to the $NO_3^-$ flux and the acid/base and tetramer equilibria. The stoichiometry of Eq. I-3 relates the flux of nitrate to the applied current. Similarly, the two equilibri-

**Table IIA. Model equations for $Ni(OH)_2$ film growth on planar electrodes. The dependent variables are $C_{Ni^{2+}}$, $C_{NO_3^-}$, $C_{H^+}$, $C_{OH^-}$, $C_{Ni_4(OH)_4^{4+}}$, and $\phi$.**

| $x = \infty$ | | $0 < x < \infty$ | |
|---|---|---|---|
| Diffusion layer-electrolyte interface | | Diffusion layer | |
| $C_{Ni^{2+}} = C^o_{Ni^{2+}}$ | [II-1] | $\frac{\partial C_{Ni^{2+}}}{\partial t} + 4\frac{\partial C_{Ni_4(OH)_4^{+4}}}{\partial t} + \nabla \cdot N_{Ni^{2+}} + 4\nabla \cdot N_{Ni_4(OH)_4^{+4}} = 0$ | [II-7] |
| $C_{NO_3^-} = C^o_{NO_3^-}$ | [II-2] | $\frac{\partial C_{NO_3^-}}{\partial t} + \nabla \cdot N_{NO_3^-} = 0$ | [II-8] |
| $C_{H^+} = C^o_{H^+}$ | [II-3] | $\frac{\partial C_{H^+}}{\partial t} - \frac{\partial C_{OH^-}}{\partial t} + \frac{\partial C_{Ni^{2+}}}{\partial t} + \nabla \cdot N_{Ni^{2+}} + \nabla \cdot N_{H^+} - \nabla \cdot N_{OH^-} = 0$ | [II-9] |
| $C_{OH^-} = C^o_{OH^-}$ | [II-4] | $K_W - C_{H^+} C_{OH^-} = 0$ | [II-10] |
| $K_{eq} C_{Ni^{2+}} C_{OH^-} = C^{1/4}_{Ni_4(OH)_4^{4+}}$ | [II-5] | $K_{eq} C_{Ni^{2+}} C_{OH^-} = C^{1/4}_{Ni_4(OH)_4^{4+}}$ | [II-11] |
| $\phi = 0$ | [II-6] | $\Sigma z_i C_i = 0$ | [II-12] |

**Table IIB. Model boundary conditions at the electrode surface.**

| $x = 0$ | | $x = 0$ | |
|---|---|---|---|
| Electrode surface (prior to precipitation) | | Electrode surface (during precipitation) | |
| $N_{Ni^{2+}} + 4N_{Ni_4(OH)_4^{+4}} = 0$ | [II-13] | $N_{OH^-} - N_{H^+} - 2N_{Ni^{2+}} - 4N_{Ni_4(OH)_4^{+4}} + \frac{s_{OH^-} i}{nF} = 0$ | [II-19] |
| $N_{NO_3^-} + \frac{s_{NO_3^-} i}{nF} = 0$ | [II-14] | $N_{NO_3^-} + \frac{s_{NO_3^-} i}{nF} = 0$ | [II-20] |
| $K_W - C_{H^+} C_{OH^-} = 0$ | [II-15] | $K_W - C_{H^+} C_{OH^-} = 0$ | [II-21] |
| $N_{OH^-} - N_{H^+} - N_{Ni^{2+}} + \frac{s_{OH^-} i}{nF} = 0$ | [II-16] | $K_{sp} - C^{1/4}_{Ni_4(OH)_4^{4+}} C_{OH^-} = 0$ | [II-22] |
| $K_{eq} C_{Ni^{2+}} C_{OH^-} = C^{1/4}_{Ni_4(OH)_4^{4+}}$ | [II-17] | $K_{eq} C_{Ni^{2+}} C_{OH^-} = C^{1/4}_{Ni_4(OH)_4^{4+}}$ | [II-23] |
| $\Sigma z_i C_i = 0$ | [II-18] | $\Sigma z_i C_i = 0$ | [II-24] |

um reactions (Eq. I-7 and I-9) are valid at the surface at all times, as shown by Eq. II-15, II-21, II-17, and II-23.

On the other hand, two sets of boundary conditions apply at the electrode surface for the $Ni^{2+}$ and $OH^-$ species. These have been derived from first principles as shown in Appendix C. Prior to precipitation, the incoming flux of nickel equals four times the flux of complex species moving away from the electrode surface, as shown in Eq. II-13. A similar expression can be written with the $OH^-$ ion which is generated in the electrochemical reaction (Eq. II-16). During precipitation, Eq. II-13 is not valid since the total flux of nickel to the electrode surface equals the rate of precipitation, $r_{ppt}$, as given by Eq. C-10. Similarly, the flux of $OH^-$ involves $r_{ppt}$ as given by Eq. C-11. This is eliminated to result in Eq. II-19. Finally, it is assumed that precipitation occurs because the surface is saturated with $OH^-$ ions. Therefore, the following equilibrium expression is included as the fifth equation

$$C^{1/4}_{Ni_4(OH)_4^{4+}} C_{OH^-} = K_{sp} \quad [6]$$

Once the unknown concentrations of species 1 to 5 are determined, the rate of deposition can be calculated using Eq. C-10. The accumulated mass of $Ni(OH)_2$ can then be determined at any given time by

$$W_{Ni(OH)_2} = \int_0^t r_{ppt} A M_{Ni(OH)_2} dt \quad [7]$$

where $A$ is the area of the electrode used in the experiments (see Ref. 2), $M_{Ni(OH)_2}$ refers to the molecular weight of nickel hydroxide, and $t$ refers to the time from the start of the experiment. The efficiency of the deposition process $\varepsilon_{OH^-}$, (based on the utilization of $OH^-$ ions) can be calculated based on the ratio of the average deposition rate (left side of Eq. 8) to the rate calculated from Faraday's law as

$$\frac{W_{Ni(OH)_2}}{t} = -\frac{9iAM_{Ni(OH)_2}\varepsilon_{OH^-}}{16F} \quad [8]$$

It should be noted that the 9/16 depends on assumption 7 and that a different, albeit similar, ratio exists if a reaction other than reaction I-3 occurs. This assumption is discussed in Ref. 2.

*Initial conditions and physical property data.*—Before the start of the experiment, it is assumed that bulk conditions exist throughout the diffusion layer. The initial conditions are the same as Eq. 5. Also, the model predictions require knowledge of physical properties of all species, and these have been summarized in Table III. Note that Streinz *et al.*[2] used 50 volume percent (v/o) ethanol/water solutions as the solvent, and the physical properties in this solvent are typically unknown. However, for aqueous solutions, earlier workers[9-12] have measured the solubility product for $Ni(OH)_2$ precipitation. A log $K_{sp,6}$ value of −14.7 can be calculated from the value reported by Kawai *et al.*[9] For aged solids, Gayer and Garrett[10] report the value of −17.2, and Jena and Prasad[11] report −16.0. Baes and Mesmer[3] state that the reported values suffer from a common uncertainty, the "physical state" of the $Ni(OH)_2$ solid. We interpret this to mean that the value of $K_{sp,6}$ can be experimentally obtained either from freshly precipitated $Ni(OH)_2$ or from the solubility data of aged $Ni(OH)_2$. The value of −13.8 reported by Wijs[12] and listed in Table I is often used. Literature values for the equilibrium constant for the tetramer formation are available only for dioxane-water solutions. That is, Kawai *et al.*[9] have reported the log $K_{eq}$ values for $Ni_4(OH)_4^{4+}$ formation in water as −27.32. This value equals 7.17 in molar units after using the $K_w$ of reaction I-9 (or 12.42 in the units of Table I) for reaction I-7. The alcohol/water solvent equilibrium constants shown in Table III correspond to estimates we obtained by comparing the model predictions and experimental data[2] at 2.5 mA/cm² and for a 2 *M* $Ni(NO_3)_2$ concentration, as discussed later.

**Table III. Physical data and model parameters used in the simulations.**

| | | | |
|---|---|---|---|
| Diffusion coefficient of the species (cm²/s) | | | |
| $Ni^{2+}$ | — | $0.69 \times 10^{-5}$ | (See text) |
| $NO_3^-$ | — | $1.84 \times 10^{-5}$ | (Ref. 8) |
| $H^+$ | — | $9.2 \times 10^{-5}$ | (Ref. 8) |
| $OH^-$ | — | $5.6 \times 10^{-5}$ | (Ref. 8) |
| $Ni_4(OH)_4^{4+}$ | — | $0.43 \times 10^{-5}$ | (See text) |

Bulk pH of $Ni(NO_3)_2$ solutions

| $C_{Ni(NO_3)_2}$ (*M*) | Bulk pH |
|---|---|
| 0.1 | 3.5 |
| 0.2 | 3.5 |
| 1.0 | 1.9 |
| 2.0 | 1.9 |

| | | |
|---|---|---|
| $T$ | — | 298 K |
| $K_{eq}$ | — | $2.61 \times 10^{11}$ (mol/cm³)$^{-7/4}$ |
| $K_{sp}$ | — | $1.2 \times 10^{-11}$ (mol/cm³)$^{5/4}$ |
| $M_{Ni(OH)_2}$ | — | 92.69 g/mol |

A value for the diffusion coefficient of the $Ni_4(OH)_4^{4+}$ species does not exist in the literature, and a value less than that for $Ni^{2+}$ was used. The aqueous dilute-solution diffusion coefficients shown by Newman[8] were used for the $NO_3^-$, $H^+$, and $OH^-$ species, since data on diffusivities in ethanol solutions do not exist. A value between the $0.72 \times 10^{-5}$ cm²/s reported by Pickett[13] and $0.5 \times 10^{-5}$ cm²/s reported by Hessami and Tobias[14] was used. The pH values of bulk $Ni(NO_3)_2$ in 50 v/o ethanol at 25°C have been reported earlier[2] and are found to vary between 2.4 for 2 *M* to 4.0 for 0.1 *M* solutions. The effect of ethanol on the selectivity of the electrochemical and homogenous reactions in Table I has not been reported. Note that inconsistencies may exist during pH measurements in alcohol solutions.[15]

*Solution procedure.*—The set of governing equations and boundary conditions is listed in Tables IIA and IIB, where Eq. 2 represents the flux. Thus, there are six nonlinear coupled equations which where solved numerically by combining implicit stepping and the BAND(J) subroutine developed by Newman.[16] The governing equations were written in finite-difference form using three-point and central differences as approximations of the first- and second-order derivatives accurate to $O(h^2)$. Typically, time steps of 0.01 s were used with 201 node points, and the accuracy was checked with 1001 points. The accuracy of the prediction was found to be in the third decimal place.

During the first time step, the technique used the set of boundary conditions which is valid for conditions prior to the onset of precipitation. The converged values of the concentrations were then used to check the solubility product criterion stated in Eq. 6. If the solubility product criterion was exceeded during the first time step, a smaller time step was used. Typically, the initial step size was decreased by a factor of ten until the concentrations were less than those required for precipitation. Then the integration was restarted using Eq. II-13 through II-18. Once the solubility product was equaled, the second set of boundary conditions was used to recompute the variables. Therefore, at each time step, Eq. 6 was checked, and the appropriate set of conditions was used in the program.

## Results and Discussion

The model was used to simulate the deposition conditions reported by Streinz *et al.*[2] In contrast to the predictions and data shown in Fig. 1, their electrolyte consisted of various concentrations of $Ni(NO_3)_2$ in a 50 v/o of ethanol and water. Their depositions were performed at constant current and at room temperature (23 to 25°C) on an EQCM. The electrode area was 0.2 cm², and the volume of the electrolyte was approximately 20 cm³. Thus, assumption 6 was valid even at 0.1 *M* $Ni(NO_3)_2$, since only 0.87 μmol of $Ni^{2+}$ would be deposited in 300 s at 2.5 mA/cm², (assuming the

stoichiometry of reaction I-3 and 100% deposition efficiency). Likewise, the bulk concentration of $H^+$ would decrease by only 0.87 μmol after 300 s at 2.5 mA/cm², even if the deposition efficiency were 50%. Thus, even at the relatively high pH shown by 0.1 *M* $Ni(NO_3)_2$, the bulk pH of 3.5 remains almost constant. We present first the comparison of the model predictions with the experimental data, and then we use the model to explain the fundamental phenomena occurring during the experiments. As shown below, the model predictions are consistent with the observations in Ref. 2 and show that $Ni^{2+}$ concentration has a pronounced effect on the deposition efficiencies at their reported current densities. It is shown that the deposition efficiency depends on the interaction of the electrochemical generation of $OH^-$, the flux of $OH^-$ and $Ni_4(OH)_4^{4+}$, and the values of the equilibrium constant and solubility products.

Figure 3 shows that, at a low concentration of $Ni(NO_3)_2$ of 0.2 *M*, the rate of deposition (*i.e.*, the slope of the mass gain *vs.* time) is constant and approximately proportional to the current density at all times. Note that the deposition efficiency for 0.2 *M* solutions determined using Eq. 8 is greater than 70% for all three current densities and that at this concentration the maximum $Ni_4(OH)_4^{4+}$ concentration is only 0.013 *M* [*i.e.*, 26% of the total nickel is in the form of $Ni(OH)_4^{4+}$]. It was observed that the deposition rate is not very sensitive to the value of the equilibrium constants and diffusion coefficients at these low concentrations and these relatively high current densities. Higher current densities increase deposition efficiency due to greater $OH^-$ generation, which causes precipitation to occur before the $Ni_4(OH)_4^{4+}$ species can diffuse away from the surface.

Figure 4 shows a comparison of model predictions and EQCM data for various concentrations of $Ni(NO_3)_2$ at an applied current density of 2.5 mA/cm². As before, the model predicts a linear increase in mass at low concentrations. However, the rate of deposition is strongly dependent on the $Ni(NO_3)_2$ concentration and decreases with increasing $Ni(NO_3)_2$ concentration. The rates of deposition are in good agreement with the experimental values at low concentrations where efficiencies are high [100% for 0.1 *M* $Ni(NO_3)_2$]; however, the model overpredicts the mass gain for 1 and 2 *M* $Ni(NO_3)_2$ concentrations for the parameters of Table III. With these parameters for 1.0 and 2.0 *M* solutions, the model predicts no deposition until 35 and 95 s, respectively. This delay is a result of an equilibrium concentration of the nickel tetramer species which is almost equal to 50% of the total nickel in solution (see Fig. 1a) prior to deposition. This relatively large tetramer concentration causes the model predictions to be very sensitive to the value of $K_{eq}$. For example, the predicted deposition

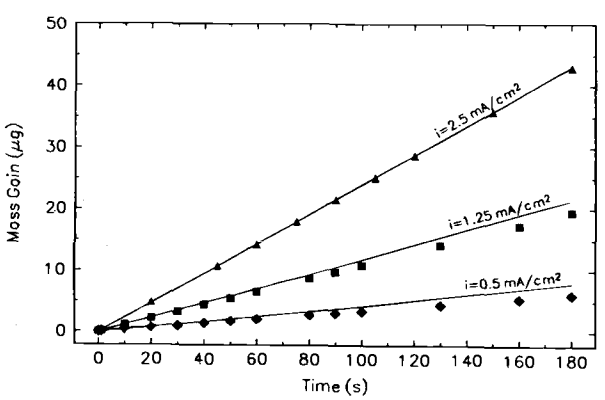


**Fig. 3. Comparison of experimental data (Ref. 2) and model predictions for 0.2 *M* $Ni(NO_3)_2$ at applied current densities of 0.5, 1.25, and 2.5 mA/cm². The model predicts a linear increase in mass and a rate which increases with current density. The rates of deposition are 2.3, 7.3, and 14.3 μg/min, and the deposition efficiencies are 71, 90, and 89% for current densities of 0.5, 1.25, and 2.5 mA/cm².**

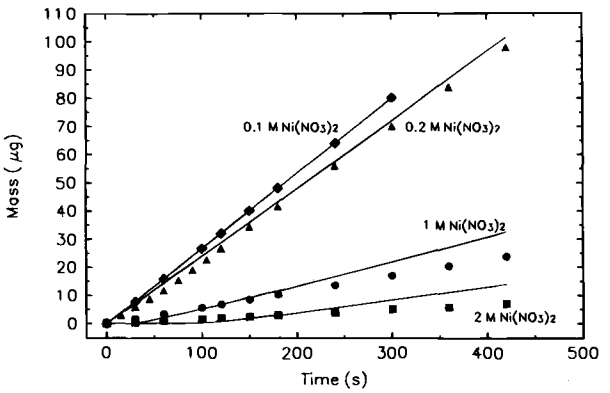


**Fig. 4. The effect of $Ni(NO_3)_2$ concentration on the comparison of experimental data (Ref. 2) and model predictions at an applied current density of 2.5 mA/cm². The predicted average rates of deposition are 16.2, 14.3, 4.5, and 2.0 μg/min for 0.1, 0.2, 1.0, and 2.0 *M* $Ni(NO_3)_2$, respectively. The experimentally observed rates were 16.2, 14.3, 3.2, and 1.0 μg/min for 0.1, 0.2, 1.0, and 2.0 *M* $Ni(NO_3)_2$, respectively.**

rate in 1 *M* $Ni(NO_3)_2$ solutions could be changed from the 4.5 μg/min of Fig. 4 to 3.06 μg/min if $K_{eq}$ was increased by 10% from that listed in Table III. Similarly, the predicted rate would increase from 4.5 μg/min to 4.62 μg/min if $K_{eq}$ was decreased by 10% with the $K_{sp}$ fixed at the value in Table III.

It must be noted that the diffusion coefficients, solubility product, and equilibrium constants in ethanol solutions are not available in the literature. Second, the effect of ethanol in the precipitation mechanism is not well understood. For these reasons, the equilibrium constant values were adjusted from those reported in the literature[9-12] to those shown in Table III. This adjustment was done by comparing the model predictions and the data at 2.0 *M* and 2.5 mA/cm² without the aid of parameter-estimation techniques. Note that the predictions are very sensitive to changes in *K* values at these conditions. It must also be noted that these values have been obtained by assuming the diffusion coefficients of all species to be independent of solution concentration and equal to their dilute-solution values. The agreement can be considered adequate, since the primary objective of this paper is to explain the observable inefficiency based on the formation of this complex species.

Figure 5 shows the model predictions of the instantaneous rate of precipitation of $Ni(OH)_2$ at 2.5 mA/cm² for the concentrations of Fig. 4. For dilute solutions (0.2 *M*), deposition begins immediately, and the rate attains a constant value from the start of the experiment. For 1 *M* solutions, the rate is zero initially and then undergoes a step change, increases, and reaches a constant value in about 35 s. For the 2 *M* solutions, the step change occurs after about 95 s. The delay in the onset of precipitation is a result of the time required for the concentration of $OH^-$ at the surface to change from the bulk pH to that consistent with the $K_{sp}$. It should be noted that the boundary conditions at the electrode surface are changed at these times as we have described.

Figure 6a shows this delay and the model predictions of the pH change for a bulk concentration of 1 *M* $Ni(NO_3)_2$ at 2.5 mA/cm². From an initial value of 1.9, the pH at the electrode rises until it equals the required value for deposition. The pH corresponding to deposition of $Ni(OH)_2$ in 50 v/o ethanol is 7.35 for 1 *M* $Ni(NO_3)_2$ and occurs at 27 s, as shown in Fig. 6a. This figure also shows that the neutralization plane moves away from the electrode surface at a rate which decreases with time from an initial value of approximately $7 \times 10^{-4}$ cm/s after 30 s. Note that for the case where a complexation reaction does not exist, the diffusion layer thickness should grow at a faster rate,

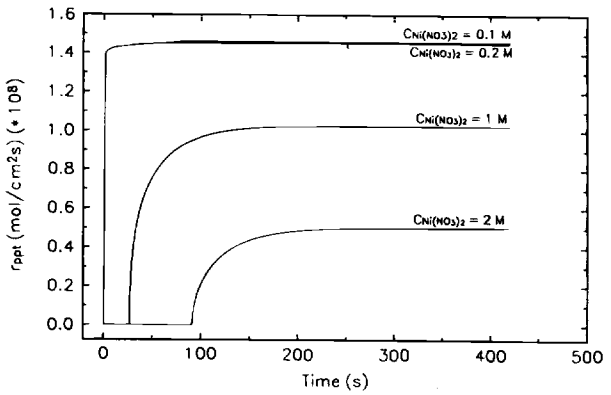


**Fig. 5. The time dependence of the rate of precipitation of $Ni(OH)_2$ in various concentrations of $Ni(NO_3)_2$ at a current density of 2.5 mA/cm². Decreasing the $Ni(NO_3)_2$ concentration (from 2 to 0.2 *M*) causes a threefold increase in the rate. In dilute $Ni(NO_3)_2$, precipitation begins immediately, and the rate attains a constant value. In concentrated $Ni(NO_3)_2$, the rate is zero initially, then increases quickly, and finally attains a steady value.**

proportional to $\sqrt{t}$. Figure 6b shows that the establishment of the required precipitation pH occurs within the first 0.5 s at a lower concentration of 0.2 *M* for 2.5 mA/cm². This is a result of two competing phenomena: First, the tetramer is a much smaller fraction of the total $Ni^{2+}$ concentration (see Fig. 1a), and thus there is a smaller concentration gradient for the movement of this intermediate species. Second, the bulk pH of 0.2 *M* $Ni(NO_3)_2$ is higher

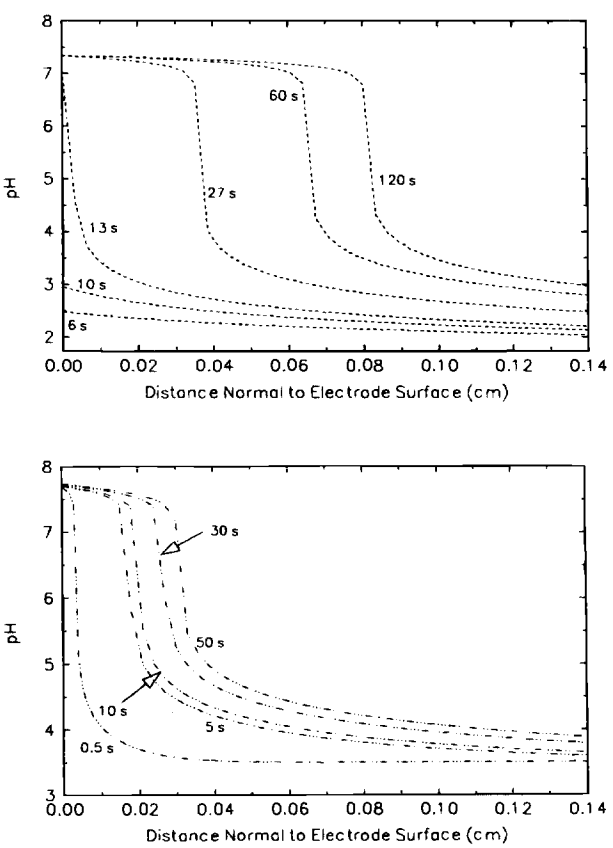


**Fig. 6. (a, top) pH profiles near the electrode surface. The profiles were obtained in 1 *M* $Ni(NO_3)_2$ at 2.5 mA/cm². The figure shows the movement of the acid/base neutralization plane away from the electrode surface as time progresses. (b, bottom) pH profiles in 0.2 *M* $Ni(NO_3)_2$ at 2.5 mA/cm².**

than that of 1 *M* $Ni(NO_3)_2$ (*i.e.*, compare 3.5 *vs.* 1.9, as shown in Table III).

Figure 7 further illustrates the model predictions at 2.5 mA/cm² for two concentrations by comparing the values of $N_1 \times 10^8$, $N_5 \times 4 \times 10^8$, and $r_{ppt} \times 10^8$ at $x = 0$. At 1 *M* $Ni(NO_3)_2$, the fluxes of $Ni^{2+}$, $Ni_4(OH)_4^{4+}$, and the rate of precipitation, $r_{ppt}$, are zero until about 13 s. At short times ($t <$ 13 s), the electrochemically generated $OH^-$ neutralizes the acidity of the solution, which raises the local pH as discussed previously. At 13 s, the fluxes become infinite and then quickly become stoichiometrically equal and opposite at ±3 mol/cm²-s until 27 s. Comparison with Fig. 6a shows that 13 s is the time after which the surface pH is constant and the time when the neutralization front begins to move away from the surface. Comparison of Fig. 7 and 6b shows that for 0.2 *M* $Ni(NO_3)_2$, the acidity is neutralized in less than 0.5 s. This short time corresponds to the nearly instantaneous start of deposition for 0.2 *M*.

Not shown in Fig. 7 is the relative contribution of diffusion and migration to the flux of $Ni_4(OH)_4^{4+}$. For 0.2 *M* $Ni(NO_3)_2$, the migration term was observed to be relatively constant at $8 \times 10^{-11}$ mol/cm²-s, but the diffusion term decreased by a factor of 20 from approximately $-4.3 \times 10^{-9}$ mol/cm²-s during the first 150 s of deposition. On the other hand, at 1 *M* $Ni(NO_3)_2$, the diffusion flux decreased by a factor of three from approximately $-3 \times 10^{-8}$ mol/cm²-s between 15 and 150 s. The migration term increased from approximately $2 \times 10^{-11}$ to $3.2 \times 10^{-10}$ mol/cm²-s during the same period. Thus, migration is not important for the concentrations of Fig. 7.

Figure 8a shows that the delay in the rate of precipitation between 15 and 27 s corresponds to the time required for the tetramer concentration to reach $10^{-2}$ *M*. After this time, the diffusion layer for the tetramer begins to grow at an initial rate of approximately $3 \times 10^{-3}$ cm/s. Once the precipitation of $Ni(OH)_2$ begins, the fluxes of $Ni^{2+}$ and $Ni_4(OH)_4^{4+}$ decrease with time, as shown in Fig. 7. Since the tetramer concentration gradient is very steep, its flux drops faster than that of $Ni^{2+}$. This can be seen in Fig. 8a, which shows that within short distances from the electrode surface, the $Ni_4(OH)_4^{4+}$ concentration steeply falls to $10^{-20}$ *M* where the pH is low. This steep gradient causes the $Ni_4(OH)_4^{4+}$ species to diffuse into the bulk. Therefore, the concentrations of all nickel species at the electrode surface are decreased. At long times, the changes in the fluxes become very small, and the rate of precipitation becomes nearly a constant. Figure 8b shows the tetramer concentration profiles in the diffusion layer for 0.2 *M* $Ni(NO_3)_2$ solutions. A comparison with Fig. 8a shows that the surface concentration of $Ni_4(OH)_4^{4+}$ is almost 100 times lower than in 1 *M* solu-

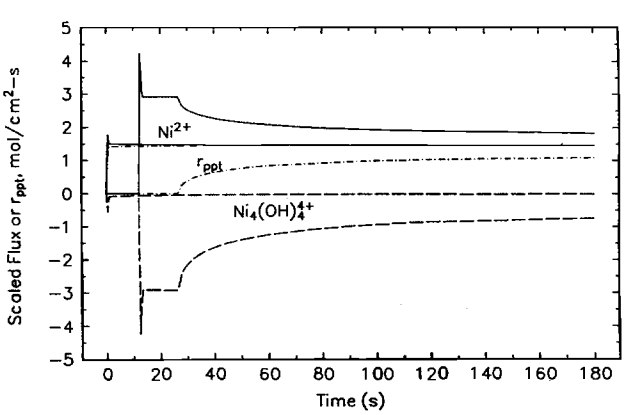


**Fig. 7. Scaled values of the flux of $Ni^{2+}$ (—), $Ni_4(OH)_4^{4+}$ (– –), and $r_{ppt}$ (– · –) at $x = 0$ for 2.5 mA/cm² and 0.2 or 1 *M* solutions. The values $N_1$ and $r_{ppt}$ are multiplied by $10^8$, and the value of $N_5$ is multiplied by $4 \times 10^8$. For 1 *M* $Ni(NO_3)_2$, the flux is zero initially and sharply rises at 13 s when the acidity of the solution is neutralized. Also at 1 *M*, $r_{ppt}$ is the total flux of all nickel species to the electrode. For 0.2 *M* solutions, $r_{ppt}$ is approximately equal to the flux of $Ni^{2+}$ since the flux of $Ni_4(OH)_4^{4+}$ is almost zero.**

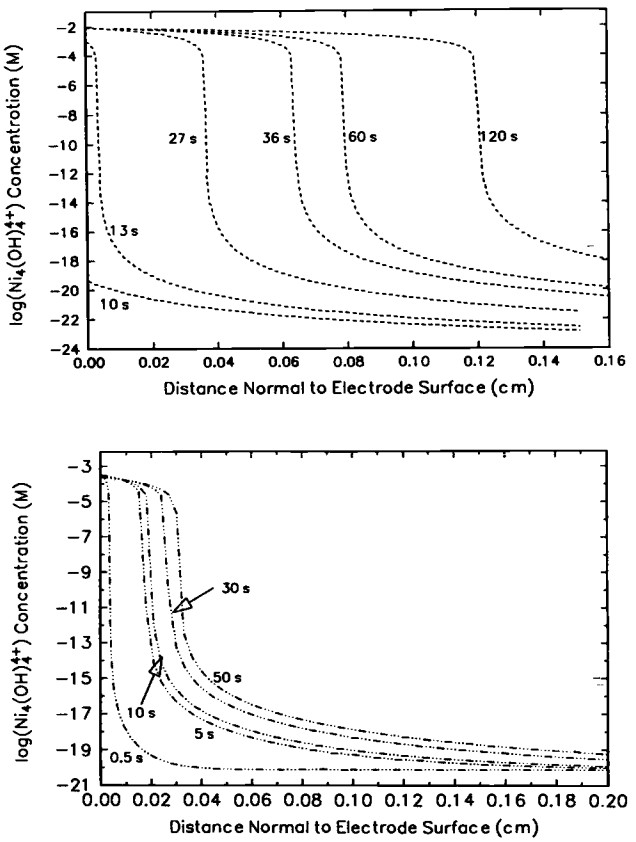


**Fig. 8. (a, top) Concentration distribution of $Ni_4(OH)_4^{4+}$ for 1 *M* $Ni(NO_3)_2$ at 2.5 mA/cm². The steep concentration gradient of $Ni_4(OH)_4^{4+}$ causes it to diffuse into the bulk. The surface concentration reaches 0.01 *M* at 27 s, and then deposition begins. (b, bottom) Concentration distribution of $Ni_4(OH)_4^{4+}$ for 0.2 *M* $Ni(NO_3)_2$ at 2.5 mA/cm². Comparison with Fig. 8a shows that the surface concentration of the $Ni_4(OH)_4^{4+}$ species is nearly 100 times lower than for 1 *M* solutions.**

tions. Furthermore, the higher initial pH of these solutions causes precipitation to start almost instantaneously.

For 1 *M* $Ni(NO_3)_2$, the bulk $H^+$ concentration is 0.0125 *M*, and Fig. 9 shows that the concentration of $H^+$ drops drastically and reaches $10^{-7}$ *M* within 15 s. The concentration of $Ni^{2+}$ during this period remains close to its bulk value throughout the diffusion layer and drops sharply only when the local pH exceeds 6.5. Therefore, the acidity of the electrolyte adjacent to the electrode is first neutralized during the initial stages of the experiment.

Due to the loss of 4 moles of hydroxyl ions for every mole of the tetramer species, the utilization of the $OH^-$ ions is greatly reduced. This efficiency, as explained in Eq. 8, can be calculated for any deposition current based on the predicted rate. Figure 10 shows the rate of deposition for a current density of 2.5 mA/cm² and $\varepsilon_{OH^-}$ at 2.5 and 5.0 mA/cm² plotted as a function of inverse $Ni(NO_3)_2$ concentration. The theoretical deposition rate, as calculated from Eq. 8, predicts a rate of 16.2 μg/min which is independent of solution concentration. This rate is observable only in 0.1 *M* solutions. In 2 *M* $Ni(NO_3)_2$, the deposition rate drops to 2 μg/min. The model predictions have been compared with the experimental data (see Ref. 2) obtained under these conditions. The variation of $\varepsilon_{OH^-}$ is also inversely related to the solution concentration. At very dilute concentrations [0.1 *M* $Ni(NO_3)_2$], $\varepsilon_{OH^-}$ is nearly equal to 1 and agrees well with the value predicted by Faraday's law. At high concentrations [2 *M* $Ni(NO_3)_2$], $\varepsilon_{OH^-}$ drops to less than 10%, and in this range the value is very sensitive to solution concentration.

## Conclusions

A mathematical model that predicts the experimentally observed inefficiencies in the deposition rates of nickel hydroxide on planar electrodes has been developed. The inefficiency in the deposition rate at high nickel concentrations ($C_{Ni(NO_3)_2} > 0.1$ *M*) is explained quantitatively by the formation of an intermediate $Ni_4(OH)_4^{4+}$ species. A two-step precipitation mechanism involving this species and proposed by Streinz *et al.*[2] has been found to be suitable in explaining the observable inefficiency. This species forms at the pH when deposition begins and diffuses into the bulk prior to deposition. The model predicts a linear increase in mass with time, as seen in the experiments for a low ratio of bulk concentration and current density. At higher ratios, the efficiency of utilization of the generated $OH^-$ drops from 100% for 0.1 *M* $Ni(NO_3)_2$ to less than 10% for 2 *M* $Ni(NO_3)_2$. Based on the agreement with experimental data, the model has been used to explain the competing phenomena occurring during the experiments. Predictions for higher temperatures and differing ethanol concentrations such as those reported recently by Streinz *et al.*[17] will require values of diffusion coefficients and equilibrium constants other than those shown in Table III. Our model could be used to estimate equilibrium and solubility product constants by fitting their deposition data. As an alternative, experiments in our laboratory focus on

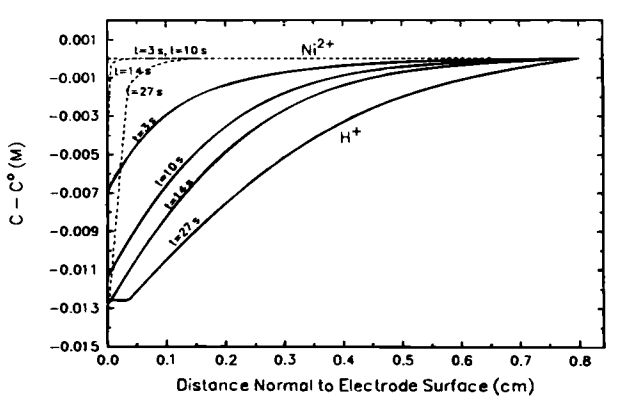


**Fig. 9. Concentration difference, $C - C^\circ$, for $H^+$ and $Ni^{2+}$ for a $Ni(NO_3)_2$ concentration of 1 *M* at 2.5 mA/cm². During the first 13 s, the electrochemically generated $OH^-$ is neutralized, causing the $H^+$ concentration at the surface to decrease while the $Ni^{2+}$ concentration remains constant. At 14 s, the $H^+$ concentration reaches $10^{-7}$ *M*, causing $Ni^{2+}$ concentration to drop due to the formation of the $Ni_4(OH)_4^{4+}$ species.**

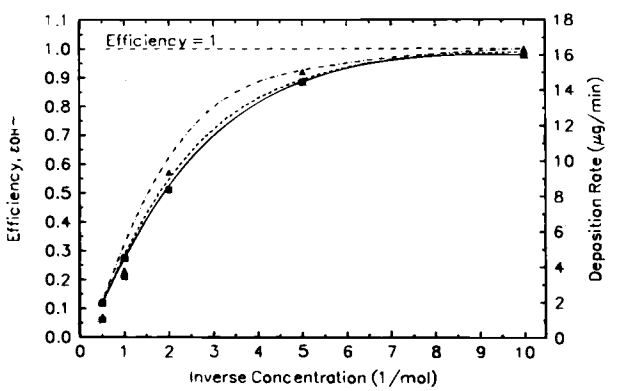


**Fig. 10. Comparison of model predictions and experimentally measured deposition rate (Ref. 2) of $Ni(OH)_2$ and $\varepsilon_{OH^-}$ (defined by Eq. 8). At 2.5 mA/cm², the rate of deposition (— and •) in dilute solutions (0.1 *M*) equals the theoretical value predicted by Faraday's law, while in 2 *M* solutions, the rate drops to 2 μg/min. $\varepsilon_{OH^-}$ is predicted at applied current densities of 2.5 (– – and ■) and 5 mA/cm² (– · – and ▲). For both current densities, higher concentrations result in lower efficiencies.**

independent measurement of these constants. This fundamental understanding of the chemistry of the deposition process will help develop better mathematical models for the impregnation of nickel electrodes.

## Acknowledgments

The authors acknowledge financial support from the Office of Research and Development of the United States Central Intelligence Agency for this project. We are also grateful for support from the Department of Energy by Cooperative Agreement DE-FCO2-91ER75666, Amendment No. A004.

Manuscript submitted Dec. 19, 1995; revised manuscript received April 15, 1996.

*The University of South Carolina assisted in meeting the publication costs of this article.*

## APPENDIX A

### Necessary Equations for Developing Fig. 1a

In this section, we describe the equilibrium equations that were solved to obtain the fraction of the total nickel that exists as $Ni^{2+}$, $Ni_4(OH)_4^{4+}$, and $Ni(OH)_2$ as a function of pH. It should be noted that the predictions of Fig. 1a neglect activity-coefficient corrections to the equilibrium and solubility-product constants. The precipitation pH divides the plot into two regions, and therefore, two sets of equations are needed.

*Case I: Prior to $Ni(OH)_2$ precipitation.*—We first make a mass balance on the total nickel in solution. All the nickel in solution exists either as its divalent ion, $Ni^{2+}$ (x) or as the $Ni_4(OH)_4^{4+}$ (y) species. If $c$ denotes the concentration of $Ni(NO_3)_2$, we can write the following mass balance

$$c = x + 4y \qquad [A\text{-}1]$$

Then we have the two equilibrium relations given by reactions I-7 and I-9, and the four unknowns are the concentrations of $Ni^{2+}$, $H^+$, $OH^-$, and $Ni_4(OH)_4^{4+}$. By fixing the pH, the other three unknowns can be determined. It must be noted that pH can be varied until a value corresponding to the precipitation pH is obtained. This value is a function of the total $Ni(NO_3)_2$ concentration, $c$.

*Case II: During $Ni(OH)_2$ precipitation.*—Once the precipitation pH is reached, nickel can also exist as $Ni(OH)_2$. Instead of Eq. A-1, we have Eq. 6 of the main section, which involves the solubility product, $K_{sp}$. Then Eq. 6 and the two equilibrium relations mentioned can be solved simultaneously by once again fixing the pH to determine the amounts of nickel present as $Ni^{2+}$, $Ni_4(OH)_4^{4+}$, and $Ni(OH)_2$.The values of $k_{eq}$ and $k_{sp}$ used for Fig. 1a are $2.6 \times 10^{12}$ $(mol/cm^3)^{-7/4}$ and $1.2 \times 10^{-11}(mol/cm^3)^{5/4}$, respectively.

## APPENDIX B

### Procedure for Measurement of pH of Aqueous $Ni(NO_3)_2$ Solutions

Fresh solutions of aqueous $Ni(NO_3)_2$ (Malinckrodt, analytical reagent grade) of concentrations ranging from 0.5 $M$ to 4.0 $M$ were prepared. A water bath was used to maintain the solutions at the desired temperature during pH measurements. The pH electrode (ROSS® type from Orion Research) was initially calibrated in standard buffer solutions of pH 4, 7, and 10. For measurements at higher temperatures, the electrode was recalibrated at the desired temperature. The pH reading was allowed to stabilize before recording. Replicates of data were taken for checking accuracy, and the averages of these values have been plotted in Fig. 1b.

## APPENDIX C

### Development of Model Equations at the Electrode Surface

This section discusses the development of model equations at the electrode surface which have been listed in Table II of the main section.

*Case I: Prior to $Ni(OH)_2$ precipitation.*—We first make a mole balance for each of the five species [*i.e.*, $Ni^{2+}$, $NO_3^-$, $H^+$, $OH^-$, and $Ni_4(OH)_4^{4+}$] considering reactions I-3, I-7, and I-9 listed in Table I. The numbered subscripts, j, denote reactions I-7 and I-9 in Table I. The rates of homogenous reactions ($r_{i,j}^*$) are written now in terms of per unit surface area of the electrode.

| Species | Mole balance at $x = 0$ | |
|---|---|---|
| $Ni^{2+}$ | $N_{Ni^{2+}} - r_{1,7}^* = 0$ | [C-1] |
| $NO_3^-$ | $N_{NO_3^-} = -\dfrac{s_{NO_3^-} i}{nF}$ | [C-2] |
| $H^+$ | $N_{H^+} - r_{3,9}^* = 0$ | [C-3] |
| $OH^-$ | $N_{OH^-} - r_{4,7}^* - r_{4,9}^* + \dfrac{s_{OH^-} i}{nF} = 0$ | [C-4] |
| $Ni_4(OH)_4^{4+}$ | $N_{Ni_4(OH)_4^{4+}} - \dfrac{r_{5,7}^*}{-r_{5,7}^*} = 0$ | [C-5] |

Next, since the rates of reaction are unknown values, they should be eliminated. That is, since $r_{1,7}^* = -4r_{5,7}^*$, adding Eq. C-1 and C-5 gives the total balance for nickel in solution (see Eq. II-13 in Table IIB)

$$N_{Ni^{2+}} + 4N_{Ni_4(OH)_4^{4+}} = 0 \qquad [C\text{-}6]$$

Similarly, since $r_{4,9}^* = r_{3,9}^*$ and $r_{4,7}^* = r_{1,7}^*$, the expression can be obtained for $OH^-$ by combining Eq. C-1, C-3, and C-4 to obtain Eq. II-16

$$N_{OH^-} - N_{H^+} - N_{Ni^{2+}} + \frac{s_{OH^-} i}{nF} = 0 \qquad [C\text{-}7]$$

The two equilibrium expressions corresponding to reactions I-7 and I-9, the electroneutrality relation given by Eq. II-18, and Eq. C-2 complete the set of six equations for the boundary conditions prior to precipitation.

*Case II: During $Ni(OH)_2$ precipitation.*—When the concentrations of $Ni_4(OH)_4^{4+}$ and $OH^-$ equal or exceed those corresponding to the solubility product of reaction I-8, precipitation conditions exist. Then, Eq. C-4 and C-5 need to be modified to include the precipitation rate, $r_{ppt}$. These flux expressions for the $OH^-$ and $Ni_4(OH)_4^{4+}$ species are rewritten in Eq. C-8 and C-9

| Species | Mole balance at $x = 0$ | |
|---|---|---|
| $OH^-$ | $N_{OH^-} - r_{4,7}^* - r_{4,9}^* + r_{ppt} + \dfrac{s_{OH^-} i}{nF} = 0$ | [C-8] |
| $Ni_4(OH)_4^{4+}$ | $N_{Ni_4(OH)_4^{4+}} - r_{5,7}^* + \dfrac{r_{ppt}}{4} = 0$ | [C-9] |

Equation C-1 and C-9 can be combined to give

$$N_{Ni^{2+}} + 4N_{Ni_4(OH)_4^{4+}} = -r_{ppt} \qquad [C\text{-}10]$$

Also, Eq. C-1, C-3, and C-8 can be combined to give

$$N_{OH^-} - N_{H^+} - N_{Ni^{2+}} + \frac{s_{OH^-} i}{nF} = -r_{ppt} \qquad [C\text{-}11]$$

The rate of precipitation can be eliminated by subtracting Eq. C-10 from C-11, which results in Eq. II-19 in Table II. The set of six equations required for the six unknowns is completed by using three equilibria corresponding to reactions I-7 through I-9, Eq. C-2, and the electroneutrality expression for the solution potential, Eq. II-24.

## LIST OF SYMBOLS

| | |
|---|---|
| $A$ | area of the EQCM electrode, 0.2 $cm^2$ |
| $C_i$ | concentration of species i, $mol/cm^3$ |
| $C^\circ$ | bulk or initial concentration, $mol/cm^3$ |
| $D_i$ | diffusion coefficient of species i, $cm^2/s$ |
| $F$ | Faraday's constant, 96,487 C/mol |
| $i$ | applied cathodic current density, $A/cm^2$ |
| $K_W$ | ionic product for water equilibrium, $(mol/cm^3)^2$ |
| $K_{eq}$ | equilibrium constant for reaction I-7, $(mol/cm^3)^{-7/4}$ |
| $K_{10}$ | equilibrium constant for reaction I-10, $cm^3/mol$ |
| $K_{11}$ | equilibrium constant for reaction I-11, $mol/cm^3$ |
| $K_{sp,6}$ | solubility product for $Ni(OH)_2$ precipitation for reaction I-6, $(mol/cm^3)^3$ |

$K_{sp}$ solubility product for $Ni(OH)_2$ precipitation for reaction I-8, $(mol/cm^3)^{5/4}$
$M_{Ni(OH)_2}$ molecular weight of $Ni(OH)_2$, 92.7 g/mol
$N_i$ flux of species i, $mol/cm^2$-s
$n$ number of electrons in reaction I-3
$R$ gas constant, 8.314 J/mol K
$R_i$ net homogenous production of species i from all the reactions, $mol/cm^3$-s
$r_{i,j}$ rate of production of species i from reaction j, $mol/cm^3$-s
$r^*_{i,j}$ rate of production of species i at the electrode surface from reaction j, $mol/cm^2$-s
$r_{ppt}$ rate of precipitation of $Ni(OH)_2$ at the electrode surface,$mol/cm^2$-s
$s_i$ stochiometric coefficient of species i
$T$ temperature, K
$t$ time, s
$U^\theta$ standard potential for reactions I-1 through I-5, V
$W_{Ni(OH)_2}$ mass of $Ni(OH)_2$ deposited, g
$x$ spatial distance normal to the electrode surface, cm

Greek

$\epsilon_{OH^-}$ efficiency of $OH^-$ utilization
$\phi$ solution potential, V

Subscripts

i species involved in the various reactions (1, 2, 3, 4, and 5)
1 $Ni^{2+}$
2 $NO_3^-$
3 $H^+$
4 $OH^-$
5 $Ni_4(OH)_4^{4+}$

## REFERENCES

1. S. Gross, *Review of Electrochemical Impregnation for Ni-Cd Cells*, Boeing Aerospace Co. Report, JPL Contract 953984 WO 342-46 (1977).
2. C. C. Streinz, A. P. Hartman, S. Motupally, and J. W. Weidner, *This Journal*, **142**, 1084 (1995).
3. C. F. Baes and R. E. Mesmer, *The Hydrolysis of Cations*, p. 242-247, John Wiley & Sons, Inc., New York (1976).
4. S. I. Cordoba-Torresi, C. Gabrielli, A. Hugot-LeGoff, and R. Torresi, *This Journal*, **138**, 1548 (1991).
5. D. F. Pickett and J. T. Maloy, *ibid.*, **125**, 1026 (1978).
6. D. M. MacArthur, *ibid.*, **117**, 730 (1970).
7. D. Bernardi, Ph.D. Thesis, University of California, Berkeley (1986).
8. J. Newman, *Electrochemical Systems*, 2nd ed., Prentice Hall, Inc., Englewood Cliffs, NJ (1991).
9. T. Kawai, H. Otsuka, and H. Ohtaki, *Bull. Chem. Soc. Japan*, **46**, 3753 (1973).
10. K. H. Gayer and A. B. Garrett, *J. Am. Chem. Soc.*, **71**, 2973 (1949).
11. P. K. Jena and B. Prasad, *J. Indian Chem. Soc.*, **33**, 122 (1956).
12. H. J. De Wijs, *Rev. Trav. Chim.*, **44**, 663 (1925).
13. D. J. Pickett, *Electrochemical Reactor Design*, p. 99, Elsevier Scientific Publishing Co., Amsterdam (1979).
14. S. Hessami and C. W. Tobias, *This Journal*, **136**, 3611 (1989).
15. R. G. Bates, M. Paabo, and R. A. Robinson, *J. Phys. Chem.*, **67**, 1833 (1963).
16. J. Newman, *Ind. Eng. Chem. Fundam.*, **7**, 514 (1968).
17. C. C. Streinz, S. Motupally, and J. W. Weidner, *This Journal*, **142**, 4951 (1995).